ACS APPLIED MATERIALS & INTERFACES

Letter

www.acsami.org

Spatially Resolved Energy Transfer in Patterned Colloidal Quantum Dot Heterostructures

Ferry Prins, Areza Sumitro, Mark C. Weidman, and William A. Tisdale*

Department of Chemical Engineering, Massachusetts Institute of Technology, 77 Massachusetts Avenue, Cambridge, Massachusetts 02139, United States

ABSTRACT: Spatial uniformity is a key consideration in high-resolution displays and light-emitting structures fabricated from colloidal quantum dots (QDs). We report spatially and spectrally resolved transient photoluminescence measurements of laterally patterned QD heterostructures. We show, using a microcontact printing technique, that spatially uniform energy transfer can be achieved in a QD donor−acceptor bilayer system, highlighting the promising potential of colloidal QDs as flexible photonic components in next-generation optoelectronic technologies.

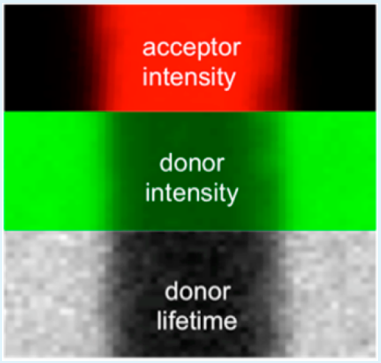

KEYWORDS: *colloidal quantum dots, energy transfer, microcontact printing, solar cells, LEDs*

Colloidal quantum dots (QDs) have emerged as powerful building blocks for next-generation optoelectronic and photonic technologies. These semiconductor nanocrystals profit from efficient luminescence, tunable and narrow emission spectra, and solution processability.[1] Recent demonstrations of their potential include multicolored lasing with single exciton optical gain,[2,3] QD-LEDs surpassing 18% efficiency,[4−6] multicolored displays,[7,8] QD-photodetectors with sensitivity across the visible and near IR frequency range,[9−11] and QD solar cells exceeding 7% efficiency.[12,13] Meanwhile, commercialized products using QDs are already entering the consumer market with the recent launch of QD LCD TVs.[14]

The size tunable properties of QDs and their narrow spectral emission allow for high-resolution band gap engineering. Using carefully chosen combinations of QDs, multistep down conversion of excitonic energy has been achieved, resulting in wider color gamuts in LED[15,16] and display technologies.[8] Alternatively, cascaded bandgap structures have been constructed to promote directional energy flow in QD materials and improve the charge collection in QD photovoltaic devices.[17−19] The mechanism of excitonic energy transfer between layers of different sized quantum dots has been studied using spectrally resolved transient spectroscopy.[16,18,20−22] Energy transfer is thought to be mediated by dipole−dipole interactions between neighboring QDs, where large bandgap dots act as donors to smaller bandgap acceptor dots.[23−25] Efficient transfer requires spectral overlap between donor and acceptor, as well as small spacing between the nanocrystals. To date, the studies of the energy transfer efficiency in QD materials have been limited to large-area ensemble measurements. However, one of the key conditions for lighting and display applications is spatial uniformity. Here, we report spatially and spectrally resolved transient photoluminescence measurements of patterned quantum-dot heterostructures. We show, using a microcontact printing technique, that efficient and spatially uniform energy transfer can be achieved in a QD donor−acceptor bilayer system.

In this study, we use core−shell CdSe/CdZnS QDs (QD Vision Inc.) of different sizes to act as donors and acceptors. Details of the quantum dot synthesis can be found in the paper by Dang et al.[3] The QDs are capped with short aromatic ligands in order to minimize the interdot distance at the interface and thereby promote efficient energy transfer. The donor layer is composed of green emitting ($\lambda \approx 550$ nm) QDs 4.0 nm in diameter, whereas the acceptor layer consists of slightly larger, 5.5 nm QDs which emit in the red ($\lambda \approx 600$ nm). The sizes were chosen such that large spectral overlap between donor emission and acceptor absorption exists. Figure 1a shows the absorbance and emission spectra of the acceptor overlaid with the emission spectrum of the donor. The donor emission is close to resonance with the second absorption peak of the acceptor.

A schematic of the different steps in the sample preparation is displayed in Figure 1b. First, a densely packed monolayer of QDs is formed using a liquid−air deposition technique.[26] For this, 2.5 mL of diethylene glycol (DEG, Sigma Aldrich) was placed in a square Teflon cup ($20 \times 20 \times 20$ mm^3). Consecutively, 75 μL of 0.5 mg/mL QDs in toluene was carefully deposited on top of the DEG surface. After evaporation of the toluene, a dense monolayer of QDs is

Received: January 10, 2014
Accepted: February 24, 2014
Published: February 24, 2014

 © 2014 American Chemical Society dx.doi.org/10.1021/am500197n | ACS Appl. Mater. Interfaces 2014, 6, 3111−3114

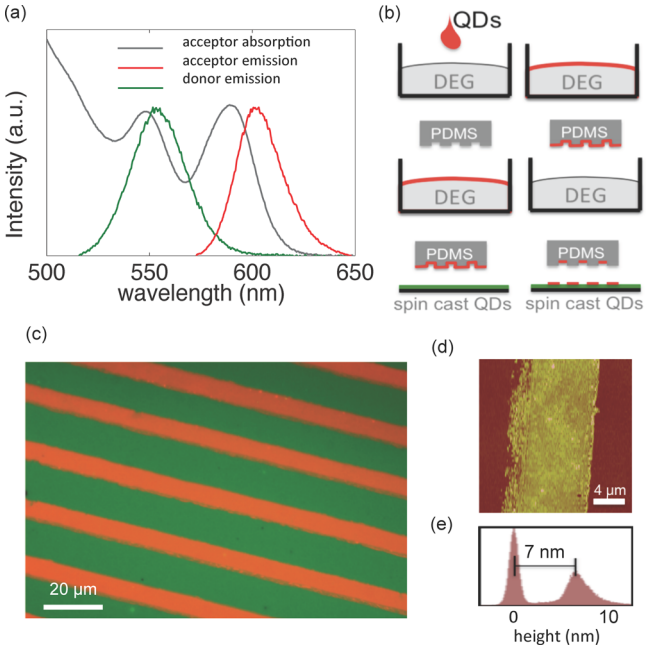

Figure 1. (a) Absorbance (gray) and emission (red) spectra of the acceptor shown with the emission spectrum of the donor (green), illustrating the spectral overlap between donor emission and acceptor absorption. (b) Densely packed monolayer of QDs is formed on top of a diethylene glycol (DEG) surface using a liquid air deposition technique (top row). This monolayer is used to ink a PDMS stamp, patterned in 10 μm wide bars with a 20 μm pitch (middle row). The inked stamp is then brought into contact with a spin-cast film of different-sized QDs to transfer the monolayer and form a patterned donor–acceptor interface (bottom row). (c) Fluorescence microscopy image of an acceptor-on-donor sample, showing well-defined stripes of red QDs on top of green QDs. (d) Atomic force microscopy image of one of the stripes shown in c. (e) Height histogram of the image shown in figure d, indicating that the height of the transferred film closely corresponds to a monolayer of QDs.

formed. This monolayer is used to ink a PDMS stamp, patterned in 10 μm wide bars with a 20 μm pitch.[15] The PDMS stamp is inked by carefully placing the patterned side in contact with the QD layer and dried under vacuum overnight to remove any DEG contaminant on the stamp. After drying, the stamp is brought into the N_2 glovebox. Without applying any pressure, the inked stamp is brought into contact with a spin-cast layer of QDs (1500 rpm, 60s from a 10 mg/mL QD solution in toluene). After 30 s, the stamp is peeled off in the direction parallel to the striped pattern. To avoid sample oxidation during measurements, each freshly prepared sample was packaged under inert atmosphere by sealing it face-down to a larger cleaned glass slide with two-component epoxy (ITW, Devcon).

Optical characterization of the samples was performed using a custom-built fluorescence microscope. The laser excitation source is a variable repetition rate laser diode (405 nm, LDH-D-C-405M, Picoquant) producing either continuous wave excitation, or pulses of ~1 ns at a repetition rate of 10 MHz. A collimated single mode beam is directed into the back of an inverted optical microscope (Nikon Ti–U, 20× objective, NA = 0.4) using a dichroic mirror to produce an excitation spot of approximately 800 nm in diameter, as determined from the reflected spot size. The sample is mounted on a metallic ring and placed on a two-axis piezo stage (MV2000, Nanonics Inc.) with a scan range of 80 × 80 μm. The fluorescence from the sample is collected by the same objective, focused into a spectrograph (Acton 2500, Princeton Instruments, 800 nm blaze), and diffracted by an 800 nm blaze grating. A thermoelectrically cooled CCD camera (Pixis 100, Princeton Instruments) is used to record full spectra. For spectrally resolved laser scanning microscopy, a spectral line 4 nm in width is focused on a single photon detecting avalanche photodiode (Tau-SPAD Series 150 μm, Picoquant). For time-resolved measurements, the output of the photo diode is connected to a timing module with a resolution of 4 ps (PicoHarp 300, PicoQuant), whereas the overall time resolution is limited by the laser pulse width (~1 ns).

Figure 1c shows a fluorescence microscopy image of an acceptor-on-donor sample, revealing well-defined stripes of red QDs on top of a substrate uniformly coated with green QDs. Atomic force microscopy (Veeco, Dimension 3100) across one of the stamped bars of this same sample shows a height of approximately 7 nm, corresponding to a monolayer of red acceptor dots (see Figure 1d, e). Using this method, we prepared samples of acceptor QDs stamped on spin-cast donor layers, referred to as the "acceptor-on-donor" configuration and shown schematically in Figure 2a. We also prepared samples of donor QDs stamped on spin-cast acceptor layers, referred to as "donor-on-acceptor" and is shown schematically in Figure 2f. Importantly, the patterned samples allow for a direct comparison of the donor and acceptors in the presence and absence of each other, providing an internal reference for calibrating energy transfer.

Figure 2b shows a color scale intensity map of the red acceptor emission of the acceptor-on-donor configuration. Sharp edged red lines of approximately 10 μm in width are alternated with dark areas where the acceptor layer is absent. The donor emission (Figure 2c) follows an opposite trend, with bright green areas where the acceptor is absent and dim areas in the presence of the acceptor layer. These trends are clearly illustrated by the horizontal line traces of the donor and acceptor intensities plotted in Figure 2d. The full emission spectra of two different positions on the sample are shown in Figure 2e. The observed anticorrelation between donor and acceptor emission intensities is consistent with energy transfer at the donor–acceptor interface, where the donor emission is quenched by the presence of the acceptor. However, donor quenching alone does not prove that an exciton has been transferred to the acceptor. To see if this is the case, we turn to the donor-on-acceptor configuration, for which the results are shown in Figure 2g–j. Indeed, we observe enhanced acceptor emission in the presence of the patterned donor layer, indicating that excitons have been transferred from donor to acceptor.

To distinguish energy transfer via electromagnetic coupling in the near-field from far-field emission-reabsorption, the quenching of the donor emission must be accompanied by a reduction of the donor lifetime. Using pulsed laser excitation in combination with time-correlated single-photon counting, we perform fluorescence-lifetime imaging microscopy. Figure 3a shows a color map of the $1/e$ donor lifetime of an acceptor-on-donor sample centered around one of the patterned acceptor stripes. The dotted white lines illustrate the edges of the acceptor stripe, as determined from a simultaneously recorded acceptor-emission intensity map. In the absence of the acceptor layer, the average lifetime of the spin-cast donor layer is 8.8 ± 0.3 ns and spatially homogeneous. However, in the presence of

dx.doi.org/10.1021/am500197n | ACS Appl. Mater. Interfaces 2014, 6, 3111–3114

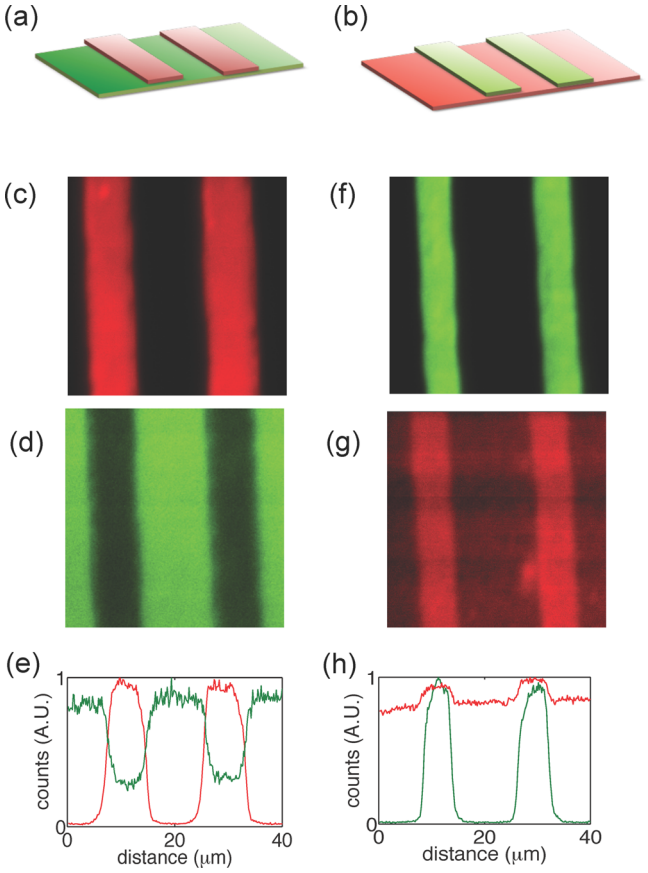

Figure 2. (a) Schematic of the acceptor-on-donor sample. (b) Fluorescence micrograph of the acceptor emission. (c) Same for donor emission. Scale bars in b and c are 10 μm. (d) Line traces of acceptor (red) and donor (green) emission. (e) Spectra of donor only region (gray) and acceptor-on-donor region (black) of the sample. (f) Schematic of the donor-on-acceptor sample. (g) Fluorescence micrograph of the acceptor emission. (h) Same for donor emission. Scale bars in g and i are 10 μm. (i) Line traces of acceptor (red) and donor (green) emission. (j) Spectra of acceptor-only region (gray) and donor-on-acceptor region (black) of the sample.

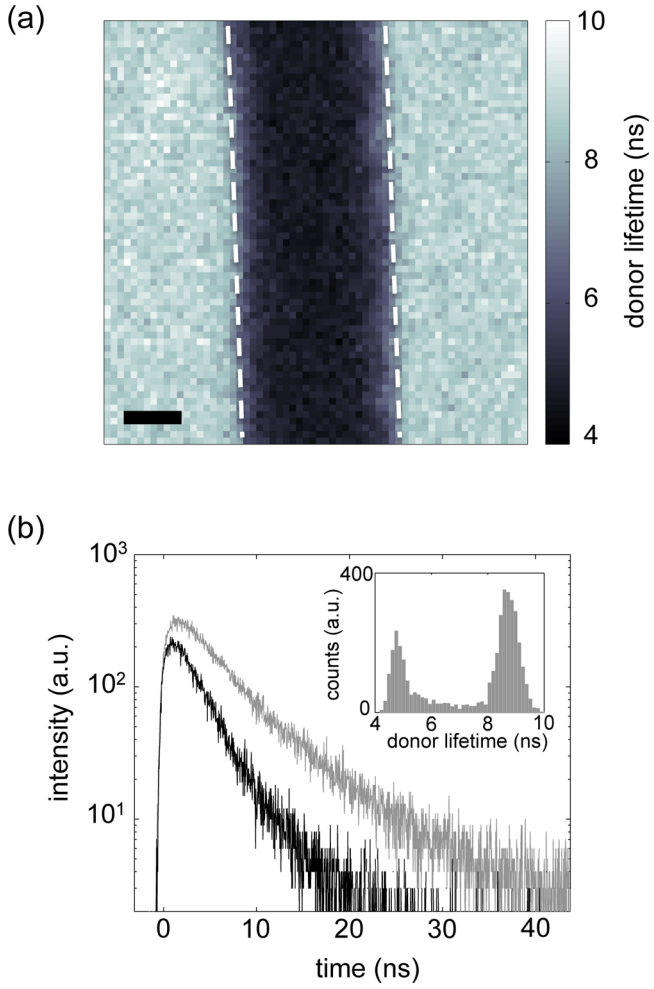

Figure 3. (a) Fluorescence lifetime micrograph of an acceptor-on-donor sample. Color scale indicates the $1/e$ lifetime of the donor channel. White dashed lines indicate the edge of the acceptor stripe. Scale bar is 2 μm. (b) Lifetime traces of the donor channel emission of a donor-only (gray line) and acceptor-on-donor (black line) part of the sample. Inset: histogram of $1/e$ donor lifetimes of the image shown in a.

the acceptor layer the lifetime of the donor is significantly reduced to an average value of 4.9 ± 0.4 ns. Figure 3b shows two representative transient fluorescence traces at donor-only and donor−acceptor positions of the sample. The inset shows a histogram of measured $1/e$ lifetimes across the image of Figure 3a. From the change in lifetime of the donor we can extract an interfacial energy-transfer efficiency, which is given by $\eta_{ET} = 1 - (\tau_{DA}/\tau_D)$, where τ_{DA} and τ_D are the lifetimes of the donor in the presence and absence of the acceptor, respectively. Using this equation we find that the local energy transfer efficiency across the stamped interface is 44 ± 9%, highlighting the spatial uniformity of the interface. The overall efficiency is comparable to values obtained in similar structures reported recently.[16]

From our spatially resolved studies, we find that our microcontact printing method results in homogeneous energy-transfer interfaces. Within the spatial resolution of our measurements (800 nm), the quenching of donor and the enhancement of acceptor emission, as well as the reduction in lifetime of the donor, show spatial variations less than 10%. These results emphasize the promising potential of colloidal QDs as flexible photonic components of next-generation optoelectronic technologies.

AUTHOR INFORMATION

Corresponding Author

*E-mail: tisdale@mit.edu.

Notes

The authors declare no competing financial interest.

ACKNOWLEDGMENTS

We thank Apoorva Murarka for assistance with the PDMS master mold fabrication. This work was supported as part of the Center for Excitonics, an Energy Frontier Research Center funded by the U.S. Department of Energy, Office of Science, Office of Basic Energy Sciences, under Award DE-SC0001088 (MIT). Atomic Force Microscopy was performed in the MIT Nanostructured Materials Metrology Laboratory within the MIT Center for Materials Science and Engineering on equipment provided by the Eni-MIT Solar Frontiers Center. A.S. acknowledges support from the MIT Energy Initiative Undergraduate Research Opportunities Program. M.C.W. acknowledges partial support from the National Science Foundation Graduate Research Fellowship Program. We thank Jonathan Steckel and Seth Coe-Sullivan of QD Vision,

Inc., for supplying QD materials. Experimental data available upon request; write to tisdale@mit.edu (W.A.T.).

REFERENCES

(1) Alivisatos, A. P. Semiconductor Clusters, Nanocrystals, and Quantum Dots. *Science* **1996**, *271*, 933−937.
(2) Klimov, V. I.; Mikhailovsky, A. A.; Xu, S.; Malko, A.; Hollingsworth, J. A.; Leatherdale, C. A.; Eisler, H.-J.; Bawendi, M. G. Optical Gain and Stimulated Emission in Nanocrystal Quantum Dots. *Science* **2000**, *290*, 314−317.
(3) Dang, C.; Lee, J.; Breen, C.; Steckel, J. S.; Coe-Sullivan, S.; Nurmikko, A. Red, Green and Blue Lasing Enabled by Single-Exciton Gain in Colloidal Quantum Dot Films. *Nat. Nanotechnol.* **2012**, *7*, 335−339.
(4) Colvin, V. L.; Schlamp, M. C.; Alivisatos, A. P. Light-Emitting Diodes Made from Cadmium Selenide Nanocrystals and a Semiconducting Polymer. *Nature* **1994**, *370*, 354−357.
(5) Coe, S.; Woo, W.-K.; Bawendi, M.; Bulović, V. Electroluminescence from Single Monolayers of Nanocrystals in Molecular Organic Devices. *Nature* **2002**, *420*, 800−803.
(6) Mashford, B. S.; Stevenson, M.; Popovic, Z.; Hamilton, C.; Zhou, Z.; Breen, C.; Steckel, J.; Bulovic, V.; Bawendi, M.; Coe-Sullivan, S.; et al. High-Efficiency Quantum-Dot Light-Emitting Devices with Enhanced Charge Injection. *Nat. Photonics* **2013**, *7*, 407−412.
(7) Wood, V.; Panzer, M. J.; Chen, J.; Bradley, M. S.; Halpert, J. E.; Bawendi, M. G.; Bulović, V. Inkjet-Printed Quantum Dot-Polymer Composites for Full-Color AC-Driven Displays. *Adv. Mater.* **2009**, *21*, 2151−2155.
(8) Kim, T.-H.; Cho, K.-S.; Lee, E. K.; Lee, S. J.; Chae, J.; Kim, J. W.; Kim, D. H.; Kwon, J.-Y.; Amaratunga, G.; Lee, S. Y.; et al. Full-Colour Quantum Dot Displays Fabricated by Transfer Printing. *Nat. Photonics* **2011**, *5*, 176−182.
(9) Konstantatos, G.; Howard, I.; Fischer, A.; Hoogland, S.; Clifford, J.; Klem, E.; Levina, L.; Sargent, E. H. Ultrasensitive Solution-Cast Quantum Dot Photodetectors. *Nature* **2006**, *442*, 180−183.
(10) Konstantatos, G.; Badioli, M.; Gaudreau, L.; Osmond, J.; Bernechea, M.; Garcia de Arquer, F. P.; Gatti, F.; Koppens, F. H. L. Hybrid Graphene-Quantum Dot Phototransistors with Ultrahigh Gain. *Nat. Nanotechnol.* **2012**, *7*, 363−368.
(11) Prins, F.; Buscema, M.; Seldenthuis, J. S.; Etaki, S.; Buchs, G.; Barkelid, M.; Zwiller, V.; Gao, Y.; Houtepen, A. J.; Siebbeles, L. D. A.; et al. Fast and Efficient Photodetection in Nanoscale Quantum-Dot Junctions. *Nano Lett.* **2012**, *12*, 5740−5743.
(12) Gur, I.; Fromer, N. A.; Geier, M. L.; Alivisatos, A. P. Air-Stable All-Inorganic Nanocrystal Solar Cells Processed from Solution. *Science* **2005**, *310*, 462−465.
(13) Ip, A. H.; Thon, S. M.; Hoogland, S.; Voznyy, O.; Zhitomirsky, D.; Debnath, R.; Levina, L.; Rollny, L. R.; Carey, G. H.; Fischer, A.; et al. Hybrid Passivated Colloidal Quantum Dot Solids. *Nat. Nanotechnol.* **2012**, *7*, 1−6.
(14) Bourzac, K. Quantum Dots Go on Display. *Nature* **2013**, *493*, 283.
(15) Kim, L.; Anikeeva, P. O.; Coe-Sullivan, S. A.; Steckel, J. S.; Bawendi, M. G.; Bulović, V. Contact Printing of Quantum Dot Light-Emitting Devices. *Nano Lett.* **2008**, *8*, 4513−4517.
(16) Kim, T.-H.; Chung, D.-Y.; Ku, J.; Song, I.; Sul, S.; Kim, D.-H.; Cho, K.-S.; Choi, B. L.; Min Kim, J.; Hwang, S.; et al. Heterogeneous Stacking of Nanodot Monolayers by Dry Pick-and-Place Transfer and Its Applications in Quantum Dot Light-Emitting Diodes. *Nat. Commun.* **2013**, *4*, 2637.
(17) Klar, T. A.; Franzl, T.; Rogach, A. L.; Feldmann, J. Super-Efficient Exciton Funneling in Layer-by-Layer Semiconductor Nanocrystal Structures. *Adv. Mater.* **2005**, *17*, 769−773.
(18) Xu, F.; Ma, X.; Haughn, C. R.; Benavides, J.; Doty, M. F.; Cloutier, S. G. Efficient Exciton Funneling in Cascaded PbS Quantum Dot Superstructures. *ACS Nano* **2011**, *5*, 9950−9957.
(19) Kramer, I. J.; Levina, L.; Debnath, R.; Zhitomirsky, D.; Sargent, E. H. Solar Cells Using Quantum Funnels. *Nano Lett.* **2011**, *11*, 3701−3706.
(20) Crooker, S.; Hollingsworth, J.; Tretiak, S.; Klimov, V. Spectrally Resolved Dynamics of Energy Transfer in Quantum-Dot Assemblies: Towards Engineered Energy Flows in Artificial Materials. *Phys. Rev. Lett.* **2002**, *89*, 186802.
(21) Achermann, M.; Petruska, M. A.; Crooker, S. A.; Klimov, V. I. Picosecond Energy Transfer in Quantum Dot Langmuir−Blodgett Nanoassemblies. *J. Phys. Chem. B* **2003**, *107*, 13782−13787.
(22) Franzl, T.; Koktysh, D. S.; Klar, T. A.; Rogach, A. L.; Feldmann, J.; Gaponik, N. Fast Energy Transfer in Layer-by-Layer Assembled CdTe Nanocrystal Bilayers. *Appl. Phys. Lett.* **2004**, *84*, 2904.
(23) Kagan, C.; Murray, C.; Bawendi, M. Long-Range Resonance Transfer of Electronic Excitations in Close-Packed CdSe Quantum-Dot Solids. *Phys. Rev. B.* **1996**, *54*, 8633−8643.
(24) Mićić, O. I.; Jones, K. M.; Cahill, A.; Nozik, A. J. Optical, Electronic, and Structural Properties of Uncoupled and Close-Packed Arrays of InP Quantum Dots. *J. Phys. Chem. B* **1998**, *102*, 9791−9796.
(25) Koole, R.; Liljeroth, P.; de Mello Donega, C.; Vanmaekelbergh, D.; Meijerink, A. Electronic Coupling and Exciton Energy Transfer in CdTe Quantum-Dot Molecules. *J. Am. Chem. Soc.* **2006**, *128*, 10436−10441.
(26) Dong, A.; Chen, J.; Vora, P. M.; Kikkawa, J. M.; Murray, C. B. Binary Nanocrystal Superlattice Membranes Self-Assembled at the Liquid−Air Interface. *Nature* **2010**, *466*, 474−477.